ACS APPLIED MATERIALS & INTERFACES

Research Article

www.acsami.org

One-Step Patterning of Hybrid Xerogel Materials for the Fabrication of Disposable Solid-State Light Emitters

Ester Carregal-Romero,[†,‡] Andreu Llobera,*[,†] Victor J. Cadarso,[†] Margarita Darder,[§] Pilar Aranda,[§] Carlos Domínguez,[†] Eduardo Ruiz-Hitzky,[§] and César Fernández-Sanchez*[,†]

[†]Instituto de Microelectrónica de Barcelona IMB-CNM (CSIC), Campus UAB, 08193, Bellaterra, Barcelona, Spain

[‡]Estudis de Doctorat Ciència de Materials, Universitat Autònoma de Barcelona, 08193, Bellaterra, Spain

[§]Instituto de Ciencia de Materiales de Madrid, CSIC, C/Sor Juana Inés de la Cruz 3 28049 Madrid, Spain

ABSTRACT: The one-step room-temperature micropatterning of a fluorophore-doped xerogel material on silicon oxide substrates is reported. The organo-alkoxysilane precursors and organic fluorescent dyes, as well as the polymerization experimental conditions, were tailored in order to obtain a highly homogeneous transparent material suitable for photonic applications. A thorough structural characterization was carried out by Fourier transform infrared (FT-IR) spectroscopy, ^{29}Si nuclear magnetic resonance (^{29}Si NMR), thermogravimetric analysis (TGA), N_2 adsorption Brunauer–Emmett–Teller (BET) porosimetry, and confocal microscopy. These studies revealed a stable nonporous highly cross-linked polymer network containing evenly dispersed fluorescent molecules. Xerogel microstructures having thicknesses between 4 and 80 μm and height-to-width ratios between 0.04 and 4, as well as showing different geometries, from well arrays to waveguides, were patterned in a single step by micromolding in capillaries (MIMIC) soft lithographic technique. The reliability of the replication process was tested by bright-field optical microscopy and scanning electron microscopy (SEM) that show the close fidelity of the microstructures to the applied mold. The optical performance of the developed material was demonstrated by fabricating waveguides and evaluating their corresponding spectral response, obtaining absorption bands, at the expected excitation wavelengths of the corresponding fluorescent dyes and gain due to photonic re-emission (fluorescence) at their corresponding dye emission wavelengths. The hybrid xerogel material and the application of the simple fabrication technology presented herein can be directly applied to the development of cost-effective photonic components, as could be light emitters, to be readily integrated in single-use lab-on-chip devices and other polymeric microsystems.

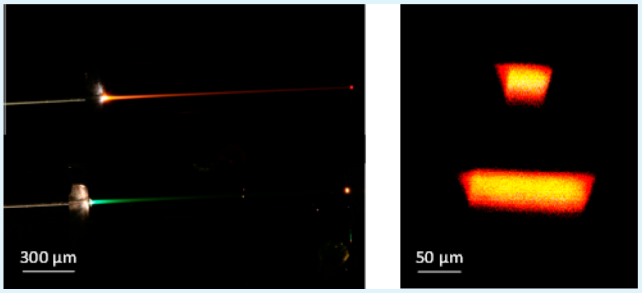

KEYWORDS: *organic–inorganic hybrids, sol–gel, xerogel, fluorophore, micromolding in capillaries, light emitter*

1. INTRODUCTION

It has been over three decades that organic–inorganic sol–gel materials have drawn a great deal of interest from the scientific community and industry.[1−5] What makes them so attractive is that these materials combine the merits of inorganic glasses and organic polymers and, moreover, they can be synthesized by a low-temperature, simple, and cost-effective process.[6] The sol–gel process consists in the formation of a polymeric network by the hydrolysis and polycondensation of metallic alkoxides. The subsequent curing and drying give rise to a xerogel material. Generally, the precursors are in the form $M(OH)_n$ and/or $M(OR)_n$, where M = Si, Ti, Zr, Al, B, ..., etc., R = (C_xH_{2x+1}) alkyl group, and n is the number of groups that can be attached to the metal.[7] Both small organic moieties and polymeric/oligomeric species can be either physically entrapped in the inorganic network (Class I sol–gel) or chemically bonded to the monomer structure (Class II sol–gel) to produce organic–inorganic hybrid network structures.[8] The sol–gel family of hybrid organic–inorganic polymers based on a silicon oxide backbone is the most widely studied and implemented. Working with alkoxysilanes, silanol groups (≡Si–OH) are generated by hydrolysis reactions in hydroalcoholic solutions usually containing an acidic or basic catalyst. Polycondensation reactions involving these groups give rise to siloxane bonds (≡Si–O–Si≡). A polysiloxane network is thus formed, and alcohol and water are generated as subproducts. The kinetics of hydrolysis/polycondensation reactions is dependent on the nature of the precursors and their ratio, as well as the working conditions that include the use of basic/acid catalysis, solvents, and temperature. A careful selection of these parameters allows one to obtain tailor-made materials with controlled properties adapted to the intended application.

The sol–gel chemistry has been shown to provide a means of entrapping a great variety of (bio)chemical species, from small

Received: July 26, 2012
Accepted: September 5, 2012
Published: September 5, 2012

   dx.doi.org/10.1021/am3014696 | ACS Appl. Mater. Interfaces 2012, 4, 5029–5037

organic molecules,[9−11] to enzymes,[12,13] living cells and other microorganisms,[14,15] and also nanoparticles[16,17] in a solid matrix while preserving their functionality. Thus, a large variety of doped hybrid organic−inorganic materials have been applied for different purposes, including the fabrication of sensor and biosensor devices[14,18−21] and the development of commercially available products,[3] such as smart drug delivery carriers for bone tissue regeneration.[22]

Sol−gel materials with very interesting properties have also been widely applied in optics and photonics.[2,23,24] Avnir's pioneering work,[25] reported over 20 years ago, demonstrated, for the first time, the incorporation of Rhodamine 6G fluorophore dye into an inorganic glass without detriment to its optical properties and performance. Since then, a wealth of sol−gel formulations have been developed and applied as passive optical sol−gel materials for applications such as anticorrosion surface coatings,[26,27] antibacterial[28] and colored coatings.[29] Also, they have shown the potential to be used as active optical matrices with photochromic properties for the development of fast optical switches and optical data storage,[30] or with luminescent properties for the fabrication of hybrid solid-state light-emitter approaches.[31,32]

The excellent properties of luminescent dye-doped sol−gel materials for the fabrication of solid-state light emitters have been clearly shown in excellent reviews by Sánchez[33] and Lebeau.[2] Dye-doped hybrid materials exhibit amplified luminescent emission at different wavelength ranges depending on the material transparency (no scattering losses), stability (aging), density (negligible optical inhomogeneity), and mechanical resistance. They should also provide the adequate environment to retain the luminescent quantum yield of the dye (lack of aggregation) and to prevent its degradation. In order to fulfill all these requirements, thorough empiric studies focused on the optimization of the hybrid xerogel matrix, the choice of the appropriate dye, and the interaction dye/matrix must be carried out.[34,35] Lasing performance of hybrid sol−gel materials doped with dyes either embedded or bound to the polymer network have been demonstrated, with the latter showing higher dye loading and thus improved performance, in terms of luminescent intensity and dye degradation.[36] However, the preparation of these materials is more laborious and is limited to dyes that could covalently react with the sol−gel matrix or required initial chemical modification of these molecules in order to get such interaction. Keeping in mind all these studies, this work shows the simple development of a tailor-made hybrid material doped with organic fluorophore dyes and its thorough characterization in order to demonstrate its suitability for the easy and cost-effective fabrication of disposable solid-state light emitters. The presented material shows the above-mentioned requirements with the added advantage of being easily synthesized and processed as microstructures of different geometries by a single-step nonphotolithographic approach without altering its material physicochemical properties and optical performance.

In most works, smart hybrid sol−gel materials are easily processed as monoliths,[37] films,[38] or powders.[39] However, one of the major advantages of sol−gel hybrids is the high versatility of the material processing, which is compatible with microfabrication techniques and enabled their application in microoptics[40,41] and integrated optics.[42−44] Depending on the chemical composition, the material can be either optically or thermally structured. In the first case, either standard UV lithography[45,46] or the promising two-photon lithography[47] have already been applied with excellent results, and structures such as optical waveguides[48] and photonic crystals[49] were fabricated. When such functionalities are not present in the material chemical composition, optically transparent, sol−gel photonic structures can still be obtained by thermally controlled processes and other lithographic techniques such as soft lithography[50] or nanoimprint lithography.[51]

Soft lithography, pioneered by Whitesides et al.,[52] includes well-known parallel nonphotolithographic approaches, some of which have been applied to the fabrication of polymeric microstructures in a one-step process. One of the competitive advantages of these techniques is related to their cost-effectiveness, simplicity, short processing time, and compatibility with a wide range of substrates and materials. Micrometer- and submicrometer-sized structures of inorganic[53,54] or functional organic−inorganic sol−gel materials[31,55] have been developed using these techniques and include orientated mesoscopic silica nanowires[53] and solid-state laser devices.[31,55] The micropatterning and nanopatterning of organic−inorganic hybrid materials has been reviewed recently, paying special emphasis on the application of soft-lithographic methods.[56]

The smart combination of soft-lithography fabrication approaches with adequate hybrid sol−gel materials make it easy to hold the low-cost assumption needed for the fabrication of disposable devices. Indeed, the objective of this work is to show how, by combining a fluorophore-doped organic−inorganic sol−gel material, thermally cured at room temperature, with the micromolding in capillaries soft lithographic technique, high-quality optical microstructures can be easily fabricated in a single step. Related previously reported approaches make use of rather complicated material synthesis approaches or photolithographic techniques, which, although they may show improved performance, make the fabrication more expensive and/or difficult to implement with other optical components.[31,55,57] The work presented here required a thorough structural and optical characterization of the material and the resulting microstructures that undoubtedly showed the potential of this approach for developing optical microstructures such as solid-state light emitters, which could be implemented in disposable polymeric photonic lab-on-chips and other microsystems.

2. EXPERIMENTAL DETAILS

2.1. Materials. Tetramethoxysilane (TMOS), methyltrimethoxysilane (MTMOS), phenyltrimethoxysilane (PhTMOS), and Rhodamine B were purchased from Sigma−Aldrich Química S.A. (Spain) and used as received. Alexa Fluor 430 carboxylic acid succinimidyl ester (Alexa) was purchased from Invitrogen (Carlsbad, CA, USA). SU-8 2005 and SU-8 2025 photocurable polymers and propylene glycol methyl ether acetate (PGMEA) developer were obtained from Microresist Technology GmbH (Berlin, Germany). The Sylgard 184 elastomer kit was obtained from Dow Corning Corp. (Midland, MI). All other chemicals were reagent-grade and used as-received.

2.2. Fluorophore-Doped Sol−Gel Synthesis. The sol solution was prepared in a fume cupboard under clean-room conditions. Some 615 μL of MTMOS, 60 μL of TMOS, and 75 μL of PhTMOS were mixed in a disposable plastic beaker, under constant stirring. Then, 2750 μL of DI water were added dropwise. These volumes gave a MTMOS:PhTMOS:TMOS molar ratio of 10:1:1 and a silanes:water molar ratio of 1:30; no catalyst was added. Molecular structures of the different components are depicted in Scheme 1. The resulting mixture was gently stirred overnight, at room temperature, until a 30% weight loss was achieved. Then, 100 μL of this sol solution was mixed with 30 μL of an aqueous solution containing either Alexa or Rhodamine B fluorophores in a concentration range from 10^{-5} M to 10^{-3} M, and

Scheme 1. Silane Precursors and Dye Chemical Structures

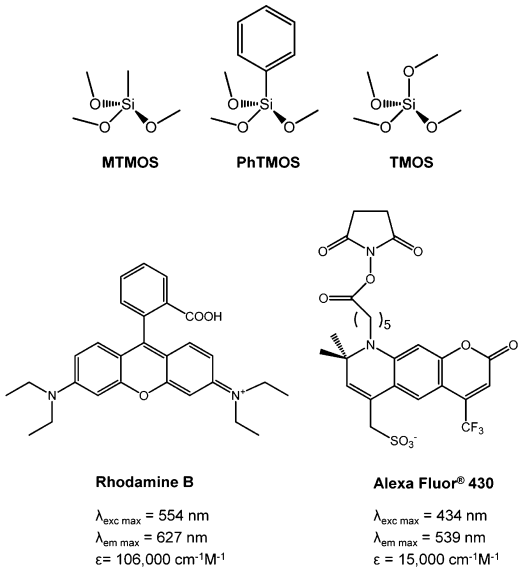

vigorously stirred in a vortex. The resulting mixtures were homogeneous, and at this point they were ready for the patterning process.

2.3. Fabrication of Masters and Stamps. Masters were fabricated with the SU-8 2005 and 2025 negative photoresists by one photolithographic process.[58] A 4-in. Si wafer (Si(100), 525 μm thick) onto which a 400-nm-thick SiO_2 was thermally grown, was cleaned with Piranha solution (fuming H_2SO_4:30% H_2O_2, 3:1 v/v). A layer of SU-8 2005 or 2025 resins then was deposited by spin-coating under different rotation speed and time conditions in order to obtain the required thicknesses. SU-8 was used for thicknesses between 4 and 25 μm, whereas SU-8 2025 was used for thicker layers. Following a bake at 95 °C for 1 h to evaporate the excess of solvent, the SU-8 was exposed to UV light through a mask. A post-exposure bake at 95 °C for 15 min was then carried out before developing the SU-8 in propylene glycol methyl ether acetate (PGMEA) that eventually revealed the masters.

The polydimethylsiloxane (PDMS) elastomer was used for the fabrication of the molds. The prepolymeric solution was prepared by mixing the Sylgard 184 elastomer with the curing agent (10:1, v/v). The mixture then was carefully poured onto the SU-8 master to cover its entire area. Air bubbles that may have been generated during the PDMS mixing and pouring process were removed under vacuum. Finally, the PDMS was cured at 80 °C for 30 min in a hot plate. The resulting mold was peeled off the master with the aid of tweezers and stored in a closed container under clean-room facilities until use.

2.4. Fabrication of Xerogel Microstructures by Micromolding in Capillaries (MIMIC). The polymer patterning was carried out on either thermally grown SiO_2/Si or glass substrates having areas between 1 and 1.5 cm^2. A previous cleaning step was done by immersion in Piranha solution for 30 min. After a rinsing step with DI water and ethanol the substrates were dried under a N_2 stream and then activated by immersion in a NH_4:H_2O_2:H_2O (1:1:5 v:v:v) solution for 10 min. This treatment improved the adherence between the exposed silanol groups in the sol–gel polymer matrix with the thus-activated silanol groups of the substrate. The PDMS mold then was placed on the substrate to establish conformal contact. Different microstructures were defined in the PDMS molds, having heights from 4 μm to 80 μm and showing different geometries and configurations. Two different MIMIC approaches were carried out. The conventional process made use of molds containing microstructures in the form of channels with opens at both ends that appear at the edge of the mold. The alternative one included the implementation of inlets and outlets on the top surface of the mold. When the former was applied, thick residual layers of the xerogel material were formed at both sides of the structures, resulting from the excess sol solution used to fill the structures. By contrast, the excess sol solution in the latter approach appeared on top of the PDMS, which, once cured, could be torn off when removing the PDMS mold. This process enables good definition of the different facets of the structures, which is important when fabricating photonic components. In both fabrication processes, a drop of fluorophore-doped sol–gel sol solution was placed at one end of the open microchannels, which were completely filled by capillary action. The PDMS/substrate system then was left undisturbed under clean-room conditions (21 °C, atmospheric pressure) for at least two days to allow the polymer to gel and dry. Once the doped xerogel was formed, the PDMS stamp was peeled off with the aid of tweezers and the microstructures were released.

2.5. Material Characterization. The following studies were carried out with nondoped and 10^{-3} M Rhodamine B-doped xerogel materials, unless stated otherwise. The latter corresponds to the material with the highest content of the fluorophore (7000:1 silane:fluorophore molar ratio in the sol solution), which was chosen in order to assess the strongest influence that the doping agent might have on the xerogel structure. This fluorophore content corresponds to a Rhodamine B concentration of 0.36 wt % in the final solid, which was estimated assuming that the monomers fully hydrolyzed and condensed to generate the polymer network and the 30% weight loss in the preparation of the sol solution was related to the evaporation of methanol, coming from the hydrolysis process of such monomers, and water. Fourier transform infrared spectroscopy (FT-IR) (Bruker IFS 66v/S spectrophotometer), ^{29}Si single-pulse (SP) solid-state magic angle spinning nuclear magnetic resonance (MAS NMR) (Bruker Avance 400 spectrometer), thermogravimetric analysis (TG-DTA) (Seiko SSC/5200), N_2 adsorption BET porosimetry (Micromeritics ASAP 2010 analyzer), and confocal microscopy studies (Leica TCS SP2 confocal microscope equipped with a HC PL APO CS 10.0× UV objective with a 0.40 numerical aperture and a diode UV 405-nm laser as the light source) were carried out in order to elucidate the structural properties of the resulting doped polymer matrix. For the ^{29}Si MAS NMR analysis, the xerogel materials were obtained in bulk, ground, and sieved to get a particle size below 150 μm. They then were spun at 10 kHz, and the spectrometer frequency was set to 79.49 MHz. Chemical-shift values were referenced to tetramethylsilane (TMS). Spectra were recorded using a single-pulse sequence of 5 μs pulse time and 5 s waiting between accumulations until ∼1200 accumulations were reached. For the FTIR study, the samples in powder form were prepared as pellets after dilution in KBr, and the spectra were recorded from 4000 cm^{-1} to 400 cm^{-1} with 2 cm^{-1} resolution. TG-DTA analysis was carried out under dynamic air atmosphere (flux of 100 mL/min) from room temperature to 850 at 10 °C/min heating rate. Textural properties were analyzed by N_2 adsorption/desorption experiments performed at 77 K after outgassing the samples at 393 K overnight. The specific total surface area and the average pore diameter were calculated by applying the Brunauer–Emmett–Teller (BET) and the Horvath–Kawazoe methods, respectively. Confocal microscopy analysis was carried out with fluorophore-doped polymer microstructures fabricated as described above. The scanned area was 600 μm × 600 μm (width × length) and pictures were taken every 0.5 μm in depth with a resolution of 8 bits. Up to 50 pictures were taken, depending on the thickness of the microstructures. The projections of the picture series were generated with Leica LAS AF software. The isosurface module of Imaris v. 6.1.0 software (Bitplane, Zürich, Switzerland) was used to reconstitute the three-dimensional (3D) models.

2.6. Characterization of the Xerogel Microstructures. Bright-field optical, fluorescence (Leica MZFLIII microscope), and scanning electron microscopy (SEM) (Zeiss LEO1530 Gemini) images were performed to test the quality of the patterning process. Optical characterization of waveguide microstructures was carried out mounting the chip in a vacuum chuck to ensure a fixed position. Two 230-μm multimode fiber optics (Thorlabs, Inc., Dachau, Germany) were employed for coupling the light in the structures and collecting it. The fiber optics were aligned with the waveguide facets with the help of micropositioners. This was possible by

fabricating the waveguides using silicon chips with a defined recessed area at both edges. Different light sources were used, depending on the fluorophore. When Alexa was applied, a blue LED light was used as light source whereas for Rhodamine B, a broadband halogen lamp (HL-2000, Ocean Optics, Dunedin, FL, USA) was used. Light collection was recorded with a microspectrometer (QE 65000-FL microspectrometer, Ocean Optics, Dunedin, FL, USA), unless stated otherwise. In order to assess the effect of the fluorophore doping component, measurements were recorded with both fluorophore-doped and nondoped (reference) xerogel waveguides.

3. RESULTS AND DISCUSSION

3.1. Synthesis and Structural Characterization of the Xerogel Material. The doped hybrid organic−inorganic xerogel was synthesized by the sol−gel technology using MTMOS, PhTMOS, and TMOS as liquid alkoxide precursors and H_2O as solvent with no catalysts.[7] MTMOS monomer was responsible for the mechanical integrity of the resulting material, also preventing the formations of cracks, fractures, or defects in the surface of the material during the drying process. In addition, it provided a strong hydrophobic character that was balanced with the presence of TMOS monomer. The role of PhTMOS is the modulation of the refractive index, which is directly related to the concentration of this monomer.[59] Two different fluorophore organic molecules were chosen, based on their absorption/emission bands, Stoke shift and proven photostability. Both Alexa Fluor 430 and Rhodamine B have been fully characterized and showed high photostability, with Alexa showing a large Stokes shift.

The preparation process of the sol solution was reproducible by keeping the room conditions (clean-room facilities) and the stirring speed constant. The weight-loss step of the sol solution was carried out in order to partly remove the water used to dissolve the silane monomers and to enable the methanol generated during the hydrolysis of the monomer methoxy groups to evaporate. In a previous work by our group,[21] it was observed that this step was required in order to get a sol solution with the required viscosity to carry out the soft lithographic patterning process and to guarantee that no loss of dimensions of the resulting polymer structures, with respect to those in the mold took place during the polymerization process.

^{29}Si NMR provides useful information about the chemical environment surrounding the Si atoms within the polymeric network. From the presented spectra shown in Figure 1A, Q^3 = XO−Si−$(OSi)_3$ signal at −101.2 ppm is ascribed to Si atoms coming from the TMOS precursor, which formed three siloxane (Si−O−Si) bonds and contain either a methoxy group or a silanol group. This signal is barely observed because of the low content of TMOS in the xerogel composition. T^n = R−Si−$(OSi)_n$ signals correspond to MTMOS and PhTMOS, which are capable to form up to three siloxane bonds, as occurs in other related systems.[10,11] The chemical shifts (T^2 −56 ppm, T^3 −65 ppm), which are typical of sol−gel silicon-based polymers,[60] are quite similar in both doped and nondoped samples. The signal at −71 ppm could also be attributed to a T^3 signal coming from Si atoms bound to aromatic moieties that appear to shift from the characteristic signal recorded when just Si atoms bound to aliphatic groups are present in the polymer matrix.[61] This signal is less intense than the one at −65 ppm and is in accordance with the PhTMOS to MTMOS molar ratios in the material composition. A slight difference in the relative T^3/T^2 areas for both materials was observed. These data provide information about the degree of condensation of the polymeric network. For the nondoped xerogel, relative

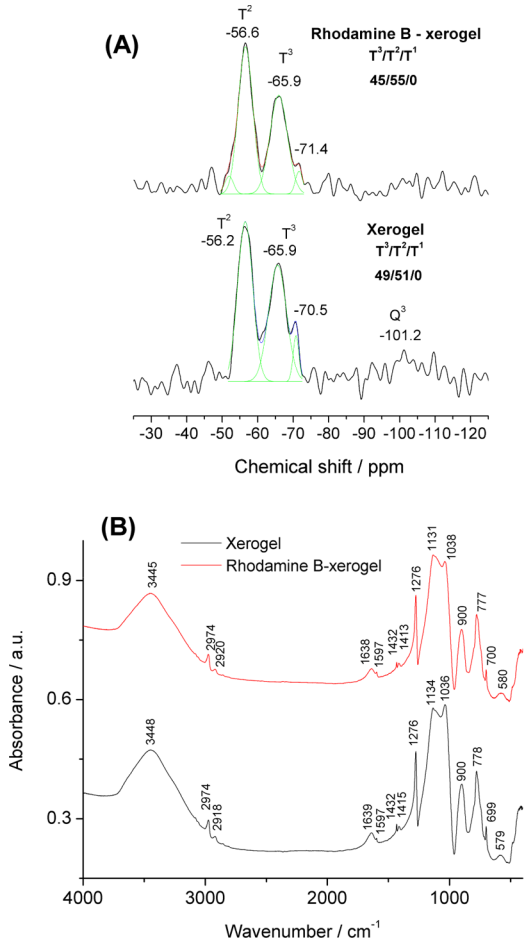

Figure 1. (A) ^{29}Si NMR and (B) FT-IR spectra of both nondoped and Rhodamine B-doped xerogels.

areas of 49/51 were calculated, which means that 49% and 51% of the Si atoms from the organotrimethoxysilanes are forming three and two siloxane bonds, respectively. The Rhodamine B-doped xerogel showed 45/55 relative values, which means that the presence of the fluorophore molecule partially impeded the formation of siloxane bonds, leading to a polymer with a slightly lower cross-linking degree. This effect caused for the inclusion of molecules into polysiloxane matrices is well-known and was previously observed for the entrapment of enzymes[21,62] and dye molecules[63] into similar polymeric cages. However, this fact affects neither the macroscopic integrity of the polymeric microstructures nor their physicochemical and optical properties, as will be shown below.

FT-IR spectra (see Figure 1B) showed the characteristic bands between wavenumbers of 1200 and 900 cm^{-1} for the stretching vibrations of Si−O bonds of the polysiloxane backbone, free silanol groups, and Si−OCH_3 groups that were not hydrolyzed during the polymerization process, for both samples. Also, a broad band in the region of 3500 cm^{-1} due to the stretching vibrations of −OH groups of Si−OH moieties is clearly visible. Both materials also showed a weak band at ∼1600 cm^{-1} corresponding to deformation vibrations of the remaining water molecules within the polymer matrix. Other bands that appear in both spectra are characteristic of bending and stretching vibrations of C−H, Si−C, and Si−CH_3 groups, as described elsewhere.[10,11] It can be stated that spectra of both nondoped and doped xerogel materials did not show

dx.doi.org/10.1021/am3014696 | ACS Appl. Mater. Interfaces 2012, 4, 5029−5037

dissimilarities that could be ascribed to the formation of different bonds due to the inclusion of the fluorophore during the polymerization process and, therefore, it did not appear to affect the polymer structure. In addition, characteristic bands for Rhodamine B that should appear between 1650 and 1750 cm^{-1}, related to the vibrations of the carbonyl group containing carboxylic moieties, cannot be observed in the FT-IR spectrum of the doped xerogel matrix, even though the material with the highest loading of the doping agent was analyzed. The reason could be the very low content of the fluorophore in the material (0.36 wt %), which cannot be detected by this spectroscopic technique.

TG-DTA analysis was carried out in order to analyze the strength of the interactions between the fluorophore molecule and the xerogel network. Figure 2 shows the TG-DTA curves

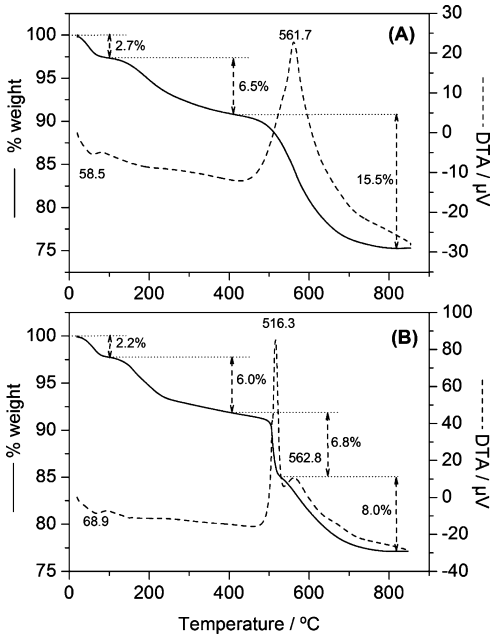

Figure 2. Thermogravimetric (solid line) and differential thermal analyses (dashed line) of (A) nondoped and (B) Rhodamine B-doped xerogel materials.

corresponding to the raw xerogel and Rhodamine-doped xerogel. The two samples showed a weight loss at ~100 °C of 2.2%–2.7%, corresponding to the complete removal of the remaining water entrapped in the matrix pores. A further weight loss of 6.0%–6.5% occurred for both xerogel and Rhodamine B–xerogel samples between 200 °C and 250 °C related to the combustion of aromatic structures and cleavage of C–C bonds. That means that this material withstands temperatures up to 200 °C. At this point, the organic components in the polymer, phenyl, and methyl groups started to degrade. The weight loss observed between 500–800 °C (~15% in both materials) can be attributed to the oxidation of pyrolytic products formed in the incomplete combustion of the organic moieties at previous stages, which remain entrapped within the dense polysiloxane matrix.[64] Although both TG curves are quite similar, a remarkable difference can be observed in the DTA curves over that temperature range. The nondoped xerogel only shows an exothermic peak centered at 562 °C, while the fluorophore-doped material shows an additional sharp and intense exothermic peak at a lower temperature of 516 °C, together with the one at 563 °C. This splitting in several decomposition stages may be related to the presence of diverse structural environments in the doped xerogel. Thus, the doped xerogel material with a lower content of Si atoms surrounded by three siloxane bonds, as determined from the ^{29}Si NMR spectra, may contain regions with a lower condensation degree, where the removal of the entrapped pyrolytic residues may be easier to occur. A similar behavior was observed in related systems of ionophore-doped MAPTS/TMOS matrixes.[65]

N_2 adsorption BET porosimetry study was carried out with nondoped and Rhodamine B-doped sol–gel materials. A very low specific surface area (~2 m^2/g) was measured for both samples that indicate a high degree of condensation and low porosity. The pore size is ~10 Å, which means that the polymer is essentially microporous. These results indicate that these materials are highly dense and, therefore, fluorophore leaching from the polymeric network can be neglected.

Confocal microscopy was carried out in order to test the dispersion of the fluorophores within the polymeric matrix. Alexa-doped xerogel waveguides were scanned in this study. Three-dimensional (3D) reconstructions of the microstructures were made, as described in the Experimental Details section, and results recorded with 100-μm-wide Alexa-doped waveguide structures are shown in Figure 3A. Similar fluorescence

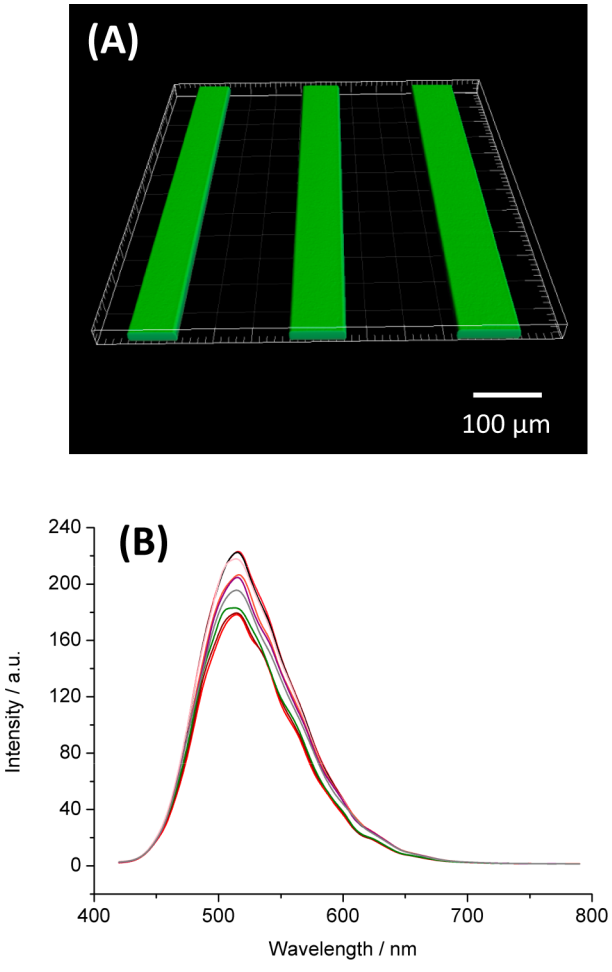

Figure 3. Optical characterization by confocal microscopy. (A) 3D reconstruction of the fluorescence intensity of Alexa-doped xerogel waveguides and (B) emission spectra recorded at nine points of the waveguides.

dx.doi.org/10.1021/am3014696 | ACS Appl. Mater. Interfaces 2012, 4, 5029–5037

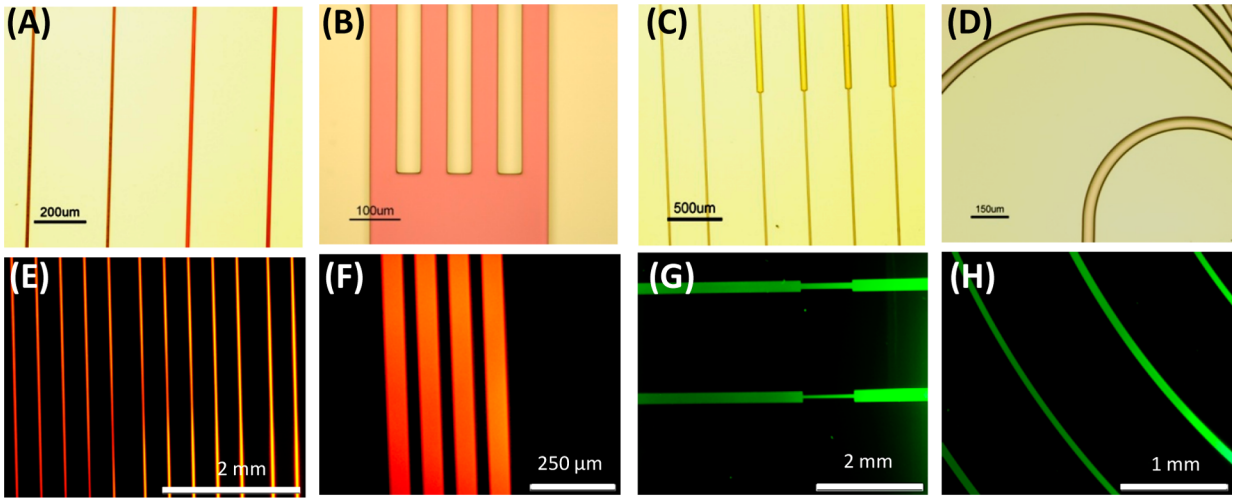

Figure 4. (A–D) Bright-field optical and (E–H) fluorescence images of microstructures fabricated using the Rhodamine B-doped (panels A, B, E, F) and Alexa Fluor-doped (panels C, D, G, H) xerogel materials. The brighter areas in images G and H come from the residual light emitted by the thick layers of the material created at the sides of the microstructures during the MIMIC fabrication process.

intensity along the structures can be observed. Also, different emission spectra at nine arbitrary points of the microstructures were also recorded and shown in Figure 3B. The mean values for the maximum fluorescence emission intensity and wavelength were 201 ± 18 (8% coefficient of variation, number of spectra = 9) and 514 ± 1 nm, respectively. These results are a good indication of the homogeneous dispersion of the fluorophores into the host matrix that is of key importance to control the optical properties of the resulting material.

3.2. Characterization of the Xerogel Microstructures. The quality of the microstructures in terms of uniformity, lack of surface defects, and reliability of the replica from the PDMS mold was tested optical and fluorescence microscopy, as well as SEM. As mentioned above, the microfabrication process applied in this work combined with the tailored xerogel material allowed the definition of structures with different geometries and sizes, with heights ranging from 4 μm to 80 μm. In order to get a high yield in the fabrication of the xerogel patterns, all the process was carried out in a controlled environment, under clean-room conditions, as pointed out previously.

In Figure 4, different bright-field optical and fluorescence microscopy images of fluorophore-doped xerogel microstructures are depicted. Rhodamine B-doped xerogel 80-μm-high waveguides showing widths between 20 μm and 100 μm (Figures 4A and 4E) and other 20-μm-high 1 × 4 multimode interference coupler (MMI) photonic structures (Figures 4B and 4F) were fabricated, as well as Alexa-doped xerogel 20-μm-high mode converter like patterns (C, G) and 4-μm-high curved waveguides (Figure 4D and 4H). These images highlight the versatility of the presented material and the microfabrication approach. Also, the inclusion of the fluorophores did not appear to affect the replication process of the xerogel microstructures. The SEM images in Figure 5 show a highly accurate reproduction of the patterns in the PDMS mold. They also evidence that the material is smooth and crack-free, thus making it a suitable candidate for photonic applications.

The fabricated microstructures were stored at room temperature for over a year without affecting their performance, with the only precaution of protecting them from light.

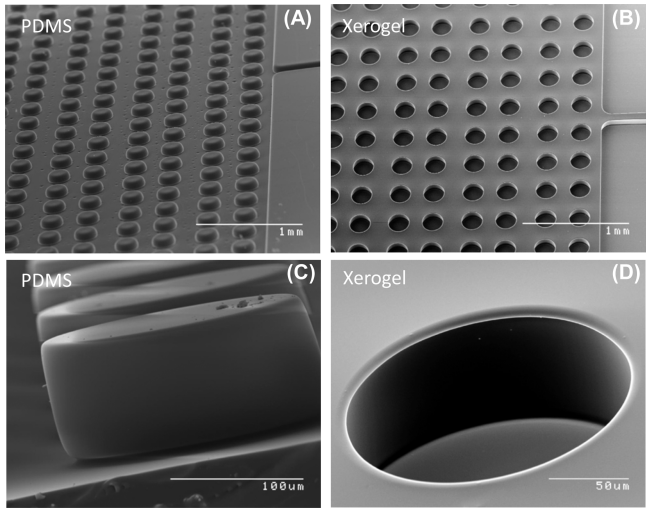

Figure 5. SEM images of the PDMS molds and the xerogel replicas: (a) array of PDMS pillars, 80 μm high × 200 μm wide; (b) array of microwells of the xerogel these being the negative replica of those pillars in the mold; (c,d) detailed images of PDMS micropillars and xerogel microwell. Samples were first sputtered with a 30-nm-thick gold layer to avoid charging effects during the analyses.

3.3. Optical Characterization of the Xerogel Material and Performance of Waveguide Microstructures. In order to demonstrate the potential of this xerogel material and the fabrication approach presented herein for the development of photonic components, an evaluation of the xerogel optical properties and a subsequent characterization of optical waveguides manufactured by MIMIC were carried out.

A study of the material transparency was carried out with the nondoped xerogel material prepared as a 2 mm-thick monolith and using a spectrophotometer. Transmittance (T) values were recorded between 200 and 800 nm, with the %T being between 94% at 300 nm (97% at 400 nm) and 99% at 800 nm and steadily decaying to 10% below 300 nm. These results evidenced that this material is transparent over the entire visible spectra and extends to the near-UV and near-IR regions.

Finally, the optical behavior of doped xerogel waveguides was assessed. Using the second approach of the MIMIC process

dx.doi.org/10.1021/am3014696 | ACS Appl. Mater. Interfaces 2012, 4, 5029–5037

described in the Experimental Details section, the waveguide facets were defined in the mold thus avoiding cumbersome cleaving post-processes that would be required using the firstly described MIMIC approach. Thus, waveguides with perfectly defined dimensions were fabricated on 1.5 cm × 1 cm Si chips coated with a 2-μm-thick thermally grown SiO_2 layer, all of them being 35 μm high and 1.5 cm long. Five different waveguides were defined on the same chip having widths of 20, 60, 100, 150, and 200 μm. These were fabricated using the nondoped xerogel as well as the Rhodamine B-doped and the Alexa Fluor-doped xerogel materials. SEM images in Figure 6

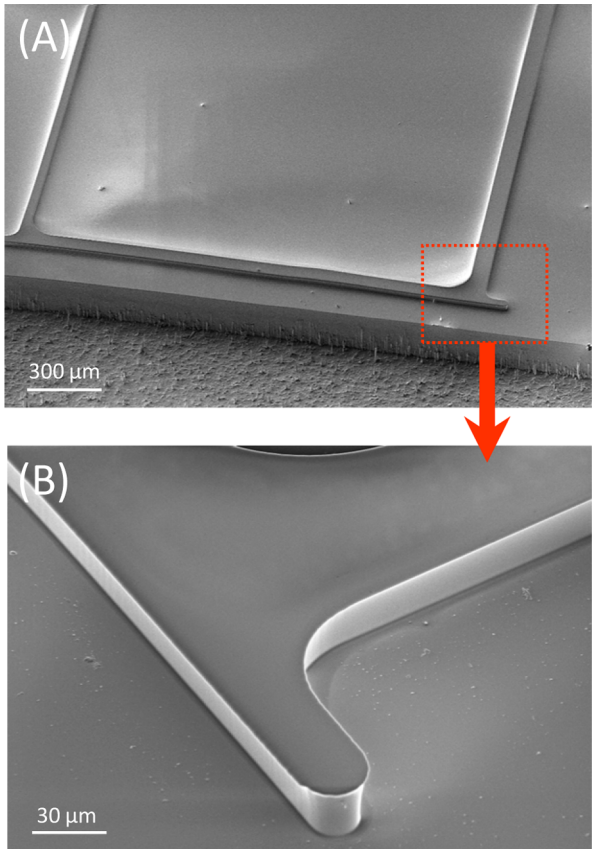

Figure 6. SEM images of (A) the fabricated waveguides and (B) close-up view of the facet end.

shows the good definition of both the waveguides and their corresponding facets. It can also be observed that a dead-end channel was defined at the outer waveguide side, with the aim of ensuring that the unstable meniscus that might be formed on the vertices of the channels were completely filled by capillary action. All of them were optically characterized using the setup described in the Experimental Details section. Figure 7A shows two waveguides fabricated with the doped xerogel material pumping light. In both cases, the output light coming from the waveguide is clearly observed. This light was imaged by replacing the output fiber with a CCD camera (Pixelfly 200 XS VGA PCO AG, Germany) and is shown in Figure 7B, which also evidenced the good confinement of the light propagating inside these structures.

Figure 8A shows the spectra recorded with a 200-μm-wide, 10^{-4} M Rhodamine B-doped xerogel waveguide and its nondoped counterpart. A strong absorption between 550 nm and 600 nm and a significant re-emission above 600 nm are

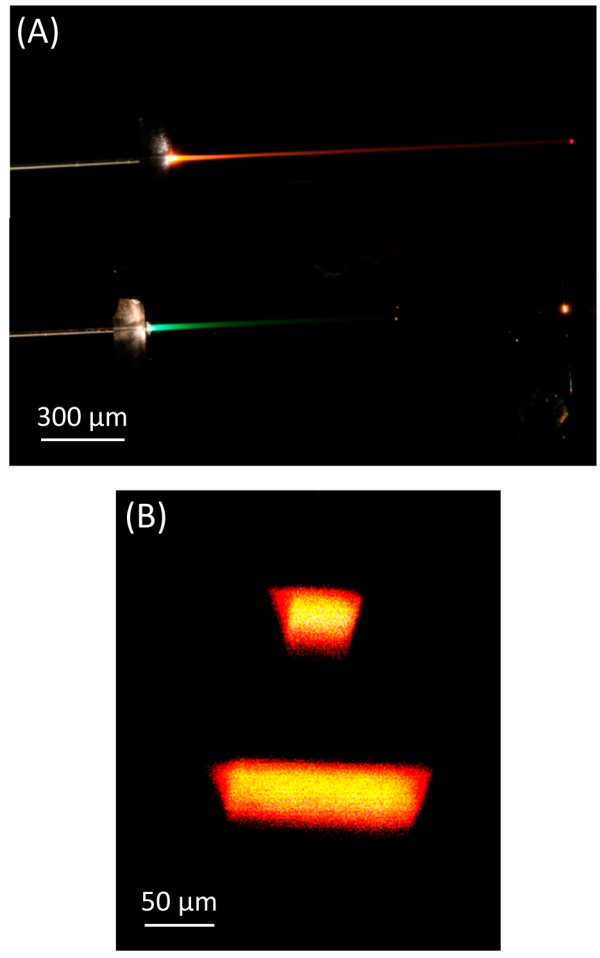

Figure 7. (A) Photograph of 60-μm-wide 10^{-4} M Rhodamine B-doped xerogel and 150-μm-wide 10^{-4} M Alexa-doped xerogel waveguides pumping light. (B) Output light recorded with both waveguides.

observed. These wavelengths match with the maximum absorption/emission of Rhodamine B ($\lambda_{absorption}$ = 554 nm, $\lambda_{emission}$ = 627 nm). In Figure 8B, the signal at lower wavelengths corresponds to the recorded output light from the excitation blue LED recorded at the end of the nondoped xerogel waveguide. At higher wavelengths, the emission band of Alexa ($\lambda_{absorption}$ = 434 nm, $\lambda_{emission}$ = 539 nm) is clearly visible. The same tests were carried out with the waveguides showing different widths on a chip, which showed that the emission intensity was proportional to the waveguide cross-sectional area.

5. CONCLUSION

A simple approach for the low-cost fabrication of polymeric photonic components based on fluorophore-doped hybrid organic−inorganic polymers was developed. A thorough characterization of the material was carried out, demonstrating its good structural and optical properties. Different microstructures were fabricated using the MIMIC soft lithography technique with high repeatability, reproducibility, and reliability in the replication of the desired dimensions. Waveguides with different dimensions were easily fabricated and optically characterized. From the results shown in this work, it can be anticipated that this material and the proposed patterning process are a suitable approach for the fabrication of disposable photonic devices. Work is in progress in order to implement

dx.doi.org/10.1021/am3014696 | ACS Appl. Mater. Interfaces 2012, 4, 5029−5037

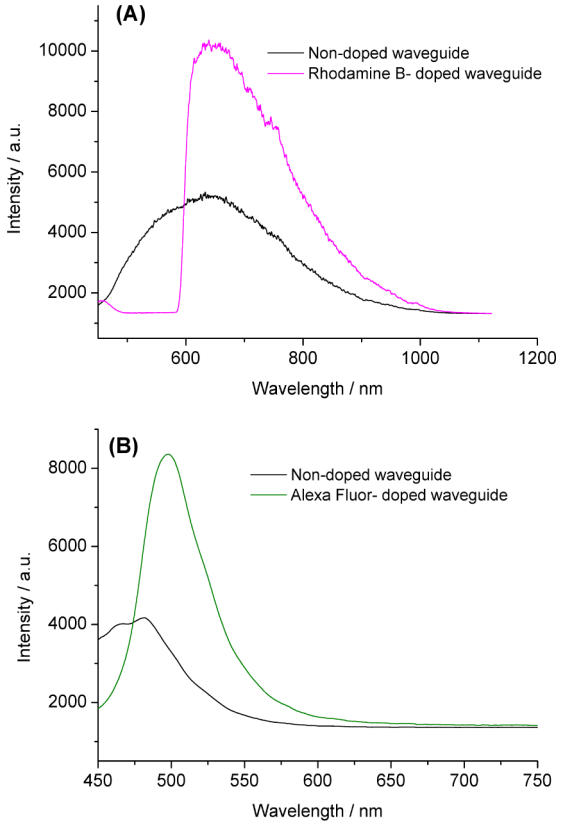

Figure 8. Spectral responses of 200-μm-wide nondoped xerogel and 10^{-4} M fluorophore-doped xerogel waveguides: (A) Rhodamine B and (B) Alexa.

fluorophore-doped xerogel solid-state light emitters in low-cost photonic lab-on-chip systems.

AUTHOR INFORMATION

Corresponding Author

*E-mails: cesar.fernandez@imb-cnm.csic.es (C.F.-S.), andreu.llobera@imb-cnm.csic.es (A.L.).

Notes

The authors declare no competing financial interest.

ACKNOWLEDGMENTS

This work was supported by the Spanish Ministry of Economy and Competitiveness (under Project Reference Nos. TEC2010-17274 and MAT2009-09960), as well as by the European Research Council, under the European Community's Seventh Framework Programme (FP7/2007-2013/ERC Grant Agreement No. 209243). We thank Dr. I. Sobrados, Dr. C. Belver, and Dr. M. Roldán for technical assistance and fruitful discussions in the NMR study, the textural characterization, and confocal microscopy analysis, respectively.

REFERENCES

(1) Novak, B. M. *Adv. Mater.* **1993**, *5*, 422−433.
(2) Lebeau, B.; Innocenzi, P. *Chem. Soc. Rev.* **2011**, *40*, 886−906.
(3) Sanchez, C.; Beleville, P.; Popall, M.; Nicole, L. *Chem. Soc. Rev.* **2011**, *40*, 696−753.
(4) Avnir, D.; Coradin, T.; Lev, O.; Livage, J. *J. Mater. Chem.* **2006**, *16*, 1013−1030.
(5) Ruiz-Hitzky, E. In *Functional Hybrid Materials*; P. Gómez-Romero Sanchez, C., Eds.; Wiley−VCH: Weinheim, Germany, 2004.
(6) Ruiz-Hitzky, E.; Aranda, P.; Darder, M.; Ogawa, M. *Chem. Soc. Rev.* **2011**, *40*, 801−828.
(7) Hench, L. L.; West, J. K. *Chem. Rev.* **1990**, *90*, 33−72.
(8) Wen, J. Y.; Wilkes, G. L. *Chem. Mater.* **1996**, *8*, 1667−1681.
(9) Zaggout, F. R. *Mater. Lett.* **2006**, *60*, 1026−1030.
(10) Aranda, P.; Jiménez-Morales, A.; Galvan, J. C.; Casal, B.; Ruiz-Hitzky, E. *J. Mater. Chem.* **1995**, *5*, 817−825.
(11) Colilla, M.; Aranda, P; Darder, M.; Ruiz-Hitzky, E. *C. R. Chim.* **2010**, *13*, 227−236.
(12) Braun, S.; Rappoport, S.; Zusman, R.; Avnir, D.; Ottolenghi, M. *Mater. Lett.* **1990**, *10*, 1−5.
(13) Avnir, D.; Braun, S.; Lev, O.; Ottolenghi, M. *Chem. Mater.* **1994**, *6*, 1605−1614.
(14) Darder, M.; Aranda, P.; Burgos-Asperilla, L.; Llobera, A.; Cadarso, V. J.; Fernández-Sánchez, C.; Ruiz-Hitzky, E. *J. Mater. Chem.* **2010**, *20*, 9362−9369.
(15) Nassif, N.; Bouvet, O.; Rager, M. N.; Roux, C.; Coradin, T.; Livage, J. *Nat. Mater.* **2002**, *1*, 42−44.
(16) Wang, M.; Xue, Y.; Lin, Z.; Huo, X.; Li, J.; Yao, X. *Mater. Lett.* **2008**, *62*, 574−576.
(17) Gurin, V. S.; Alexeenko, A. A.; Kaparikha, A. V. *Mater. Lett.* **2011**, *65*, 2442−2444.
(18) Jeronimo, P. C. A.; Araujo, A. N.; Montenegro, M. C. B. S. M. *Talanta* **2007**, *72*, 13−27.
(19) Monton, M. R. N.; Forsberg, E. M.; Brennan, J. D. *Chem. Mater.* **2012**, *24*, 796−811.
(20) Jimenez-Morales, A.; Galvan, J. C.; Aranda, P. *Electrochim. Acta* **2002**, *47*, 2281−2287.
(21) Llobera, A.; Cadarso, V. J.; Darder, M.; Domínguez, C.; Fernánez-Sánchez, C. *Lab Chip* **2008**, *8*, 1185−1190.
(22) Vallet-Regi, M.; Colilla, M.; Izquierdo-Barba, I. *J. Biomed. Nanotechnol.* **2008**, *4*, 1−15.
(23) Chaumel, F.; Jiang, H. W.; Kakkar, A. *Chem. Mater.* **2001**, *13*, 3389−3395.
(24) Yeatman, E. M.; Dawnay, E. J. C. *J. Sol−Gel Sci. Technol.* **1997**, *8*, 1007−1011.
(25) Avnir, D.; Levy, D.; Reisfeld, R. *J. Phys. Chem.* **1984**, *88*, 5956−5959.
(26) Belleville, P.; Bonnin, C.; Priotton, J. J. *J. Sol−Gel Sci. Technol.* **2000**, *19*, 223−226.
(27) Bescher, E.; Pique, F.; Stulik, D.; Mackenzie, J. D. *J. Sol−Gel Sci. Technol.* **2000**, *19*, 215−218.
(28) Saif, M. J.; Anwar, J.; Munawar, M. A. *Langmuir* **2009**, *25*, 377−379.
(29) Akamatsu, Y.; Makita, K.; Inaba, H.; Nakazumi, H.; Minami, T. *J. Sol−Gel Sci. Technol.* **2000**, *19*, 387−391.
(30) Pardo, R.; Zayat, M.; Levy, D. *Chem. Soc. Rev.* **2011**, *40*, 672−687.
(31) Yang, P. D.; Wirnsberger, G.; Huang, H. C.; Cordero, S. R.; McGehee, M. D.; Scott, B.; Deng, T.; Whitesides, G. M.; Chmelka, B. F.; Buratto, S. K.; Stucky, G. D. *Science* **2000**, *287*, 465−467.
(32) Berard, M.; Rachet, V.; Lahlil, K.; Gacoin, T.; Galaup, J. P.; Boilot, J. P. In *Photonic Metamaterials*; Noginov, M. A., Zheludev, N. I., Boardman, A. D., Engheta, N., Eds.; Proceedings of the SPIE, Vol. *6638*; SPIE: San Diego, 2007; p 66380.
(33) Sanchez, C.; Lebeau, B.; Chaput, F.; Boilot, J. P. *Adv. Mater.* **2003**, *15*, 1969−1994.
(34) Reisfeld, R.; Weiss, A.; Saraidarov, T.; Yariv, E.; Ischenko, A. A. *Polym. Adv. Technol.* **2004**, *15*, 291−301.
(35) Sanchez, C. *C. R. Chim.* **2010**, *13*, 1−2.
(36) Seifert, A.; Ladewig, K.; Schoenherr, P.; Hofmann, K.; Lungwitz, R.; Roth, I.; Pohlers, A.; Hoyer, W.; Baumann, G.; Schulze, S.; Hietschold, M.; Moszner, N.; Burtscher, P.; Spange, S. *J. Sol−Gel Sci. Technol.* **2010**, *53*, 328−341.
(37) Hoffmann, H. S.; Stefani, V.; Benvenutti, E. V.; Costa, T. M. H.; Gallas, M. R. *Mater. Chem. Phys.* **2011**, *126*, 97−101.
(38) Kazes, M.; Saraidarov, T.; Reisfeld, R.; Banin, U. *Adv. Mater.* **2009**, *21*, 1716−1720.

(39) Chen, J. P.; Lin, W. S. *Enzyme Microb. Technol.* **2003**, *32*, 801−811.
(40) Tohge, N.; Ueno, R.; Chiba, F.; Kintaka, K.; Nishii, J. *J. Sol−Gel Sci. Technol.* **2000**, *19*, 119−123.
(41) Kang, D. J.; Bae, B. S. *Acc. Chem. Res.* **2007**, *40*, 903−912.
(42) Popall, M.; Houbertz, R.; Frohlich, L.; Streppel, U.; Dannberg, P.; Westenhofer, S.; Gale, M. *Glass Sci. Technol.* **2003**, *76*, 53−58.
(43) Jabbour, J.; Calas, S.; Smaihi, M.; Gatti, S.; Etienne, P. *J. Non-Cryst. Solids* **2008**, *354*, 1001−1009.
(44) Moreau, J. J. E.; Pichon, B. P.; Arrachart, G.; Man, M. W. C.; Bied, C. *New J. Chem.* **2005**, *29*, 653−658.
(45) Bredol, M.; Schem, M. *Opt. Mater.* **2004**, *27*, 521−525.
(46) Houbertz, R.; Domann, G.; Cronauer, C.; Schmitt, A.; Martin, H.; Park, J. U.; Frohlich, L.; Buestrich, R.; Popall, M.; Streppel, U.; Dannberg, P.; Wachter, C.; Brauer, A. *Thin Solid Films* **2003**, *442*, 194−200.
(47) Houbertz, R. *Appl. Surf. Sci.* **2005**, *247*, 504−512.
(48) Bichler, S.; Feldbacher, S.; Woods, R.; Satzinger, V.; Schmidt, V.; Jakopic, G.; Langer, G.; Kern, W. *Opt. Mater.* **2012**, *34*, 772−780.
(49) Serbin, J.; Ovsianikov, A.; Chichkov, B. *Opt. Express* **2004**, *12*, 5221−5228.
(50) Fernandez-Sanchez, C.; Cadarso, V. J.; Darder, M.; Domínguez, C.; Llobera, A. *Chem. Mater.* **2008**, *20*, 2662−2668.
(51) Guo, L. J. *Adv. Mater.* **2007**, *19*, 495−513.
(52) Xia, Y. N.; Whitesides, G. M. *Angew. Chem., Int. Ed.* **1998**, *37*, 551−575.
(53) Trau, M.; Yao, N.; Kim, E.; Xia, Y. N.; Whitesides, G. M.; Aksay, I. A. *Nature* **1997**, *390*, 674−676.
(54) Marzolin, C.; Smith, S. P.; Prentiss, M.; Whitesides, G. M. *Adv. Mater.* **1998**, *10*, 571−574.
(55) Wirnsberger, G.; Yang, P. D.; Huang, H. C.; Scott, B.; Deng, T.; Whitesides, G. M.; Chmelka, B. F.; Stucky, G. D. *J. Phys. Chem. B* **2001**, *105*, 6307−6313.
(56) ten Elshof, J. E.; Khan, S. U.; Gobel, O. F. *J. Eur. Ceram. Soc.* **2010**, *30*, 1555−1577.
(57) Brusantin, G.; Della Giustina, G. *J. Sol−Gel Sci. Technol.* **2008**, *60*, 299−314.
(58) Llobera, A.; Wilke, R.; Buttgenbach, S. *Lab Chip* **2004**, *4*, 24−27.
(59) Gvishi, R.; Narang, U.; Ruland, G.; Kumar, D. N.; Prasad, P. N. *Appl. Organomet. Chem.* **1997**, *11*, 107−127.
(60) Lacan, P.; Guizard, C.; Cot, L. *J. Sol−Gel Sci. Technol.* **1995**, *4*, 151−162.
(61) Lelli, M.; Gajan, D.; Lesage, A.; Caporini, M. A.; Vitzthum, V.; Mieville, P.; Heroguel, F.; Rascon, F.; Roussey, A.; Thieuleux, C.; Boualleg, M.; Veyre, L.; Bodenhausen, G.; Coperet, C.; Emsley, L. *J. Am. Chem. Soc.* **2011**, *133*, 2104−2107.
(62) Soares, C. M. F.; dos Santos, O. A. A.; de Castro, H. F.; Itako, J. E.; de Moraes, F. F.; Zanin, G. M. *J. Non-Cryst. Solids* **2006**, *352*, 3469−3477.
(63) Ismail, F.; Schoenleber, M.; Mansour, R.; Bastani, B.; Fielden, P.; Goddard, N. J. *Analyst* **2011**, *136*, 807−815.
(64) Colilla, M.; Darder, M.; Aranda, P.; Ruiz-Hitzky, E. *J. Mater. Chem.* **2005**, *15*, 3844−3851.
(65) Jiménez-Morales, A. Sensores electroquímicos y membranas de separación iónica basados en materiales organopolisiloxánicos que incorporan compuestos ionóforos o enzimas (Electrochemical sensors and ionic separation membranes based on organopolysiloxane materials incorporating ionophores or enzymes). Ph.D. Thesis, Carlos III University, Madrid, Spain, 1999.